J Appl Electrochem (2012) 42:667–677
DOI 10.1007/s10800-012-0445-x

ORIGINAL PAPER

Design and optimization of electrochemical microreactors for continuous electrosynthesis

C. Renault · J. Roche · M. R. Ciumag · T. Tzedakis · S. Colin · K. Serrano · O. Reynes · C. André-Barrès · P. Winterton

Received: 4 January 2012 / Accepted: 3 July 2012 / Published online: 26 July 2012

Abstract The study focuses on the design and construction, as well as the theoretical and experimental optimization of electrochemical filter press microreactors for the electrosynthesis of molecules with a high added value. The main characteristics of these devices are firstly a high-specific electrochemical area to increase conversion and selectivity, and secondly the shape and size of the microchannels designed for a uniform residence time distribution of the fluid. A heat exchanger is integrated into the microstructured electrode to rapidly remove (or supply) the heat required in exo- or endothermic reactions. The microreactors designed are used to perform-specific electrosynthesis reactions such as thermodynamically unfavorable reactions (continuous NADH regeneration), or reactions with high enthalpy changes.

C. Renault
Laboratoire de Génie Chimique, Université de Toulouse, INP-ENSIACET, 31030 Toulouse, France

J. Roche · M. R. Ciumag · T. Tzedakis (✉) · K. Serrano · O. Reynes
Laboratoire de Génie Chimique, Université de Toulouse, UPS, 118, route de Narbonne, 31062 Toulouse, France
e-mail: tzedakis@chimie.ups-tlse.fr

S. Colin
Université de Toulouse; INSA, UPS, Mines Albi, ISAE; ICA (Institut Clément Ader), 135 Av. de Rangueil, 31077 Toulouse, France

C. André-Barrès
Laboratoire de Synthèse et Physicochimie des molécules d'intérêt biologique, Université de Toulouse, UPS, 118, route de Narbonne, 31062 Toulouse, France

P. Winterton
Département Langues & Gestion, Université de Toulouse, UPS, 118, route de Narbonne, 31062 Toulouse, France

Keywords Electrochemistry · Microreactors · Electrosynthesis · Fluorination · NADH regeneration · Optimization · Simulation · POISEUILLE · Pressure drop

List of symbols

C or c	Concentration (mol L^{-1})
C_p	Heat capacity of the coolant EG (2,400 $J{\cdot}kg^{-1}{\cdot}K^{-1}$)
$C_{p,j}$	Specific heat of each reactant or product j
D	Diffusion coefficient (m^2 s^{-1})
DG	Deoxy-D-glucose
DME	Dimethoxyethane
E	Potential (V)
$E_{\text{elect. } E \text{ exch.}}$	Electrical and exchanged energy, respectively
EG	Ethylene glycol
e_{bl}	Thickness of the metallic fin of the heat exchanger (m)
$Et_3N{\cdot}3HF$/TEAHF	Triethylamine trihydrofluoride
F	Faraday constant (96,485 C mol^{-1})
$F°$	Molar flux at the input and the output of the microreactor
FAD/$FADH_2$	Flavin redox mediator (oxidized and reduced forms)
FDH	Formate dehydrogenase enzyme
FDG	Fluoro-deoxy-D-glucose
g	Acceleration due to gravity 9.80665 m s^{-2}
h	Convective exchange coefficient of the coolant (W m^{-2} K^{-1})
i	Current density (A m^{-2})
k	Mass transfer coefficient (m s^{-1})
K	Equilibrium constant

k_{cat}	Rate of the enzyme catalyzed reaction (s^{-1})
$K_{m,j}$	Michaelis–Menten constants (L^{-1} mol^{-1})
L	Length of the considered "reactive" channel or microchannel segment (m)
L_{bl}	Length of the metallic fin of the heat exchanger (m)
n	Electron number
n_μ	Number of microchannels on the plate
NAD^+/NADH	Nicotinamide dinucleotide pyridinic cofactor (oxidized and reduced forms)
Nu	Nusselt number ($Nu = hL_{bl}/\lambda$)
p	Pressure (Pa)
p_{exch}	Overall perimeter of the fin section (m)
Po	Poiseuille number
Q	Charge (F mol^{-1})
Q_v	Volumetric flow rate (m^3 s^{-1})
R	Universal gas constant (8.31 J mol^{-1} K^{-1})
I	Current (A)
r_j	Rate of homogeneous reactions (mol m^{-3} s^{-1})
$r_{\chi R}$	Rate of chemical reaction (mol m^{-3} s^{-1})
S	Cross-section area of the flow channel (m^2)
S_a	Electrode active surface area (m^2)
S_{exch}	Total surface area of all the fins (m^2)
t	Time (s)
T	Absolute temperature (K)
TBAP	Bu_4NClO_4
u_{EG}	Coolant velocity (0.02 m·s^{-1})
V_{EC}	Electrolytic compartment volume (m^3)
X	Conversion of the limiting reagent
x, y, z	Axis coordinate
$\Delta_f H_j^\circ$	Standard formation enthalpy of the species j (J mol^{-1})
$\Delta_R H^\circ$	Standard reaction enthalpy (J mol^{-1})
$\Delta_R G^\circ$	Standard reaction-free enthalpy (J mol^{-1})
ΔP	Pressure drop (Pa)
ΔV	Cell voltage (V)
θ	Opening angle of the distributing and/or collecting channels (°)
λ	Coolant thermal conductivity (W m^{-1} K^{-1})
μ	Dynamic viscosity Pa s)
ν_j	Stoichiometric coefficient
ρ	Specific gravity of the coolant (1,109 kg·m^{-3})
τ	Residence time in the reactor (s)
$\overrightarrow{v}$	Fluid velocity (m s^{-1})
ϕ	Heat flux (J s^{-1})

1 Introduction

This study deals with the design and optimization (theoretical and experimental) of electrochemical microreactors for the electrosynthesis of various types of molecules with a high-added value. The microreactor is expected to operate continuously, under conditions allowing minimization of both costs and risks of the isothermal synthetic processes. A high-specific area of the electrochemically active surface increases conversion and selectivity.

2 Microreactor design and construction

2.1 Microreactor design

This part of the study concerns the design of microstructured electrodes and the incorporated heat exchanger. Their shape and size should allow a uniform residence time distribution for efficient and selective electrochemical reactions. Square or semi-circular microchannel cross-sections yield a specific surface area of at least 200 cm^{-1}.

2.1.1 Optimal geometry of the microreactor

To carry out preparative electrosynthesis of valuable adducts using microreactors able to operate under volumetric flows in the range of $1 < Q_{v\ (cm/min)}^3 < 10$, an appropriate hydraulic diameter of the microchannels is a few tens of μm. Consequently the influence of electrokinetic or electrocapillarity phenomena can be ignored in the calculations. Poiseuille's law is used to evaluate the pressure drop between the various parts of the inlet and outlet channels as well as through the microchannels [1–4]. The electrolytic compartment is lined by microgrooves cut into the solid electrode. Various shapes are possible for the electrodes, the microchannels, and the distributing/collecting channels (Fig. 1). Both the length and the width of the microchannels, as well as the openness of the distributing and collecting channels are parameters that must be optimized to improve the efficiency of the microdevice.

To propose a microdevice with a specific surface area (for the electrochemical reaction) in the range of

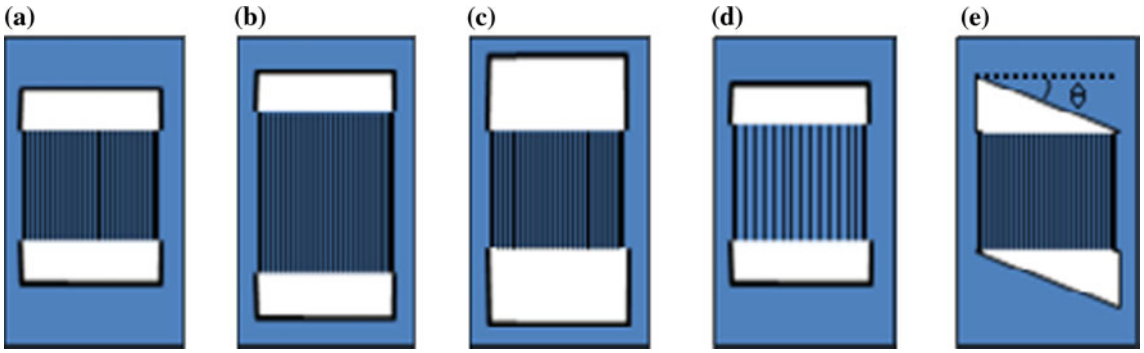

Fig. 1 Various possible shapes for microstructured electrodes. **a** Standard shape including distributing, collecting channels, and reaction microchannels. **b** Longer reaction microchannels. **c** Larger distributing and collecting channels. **d** Larger reaction microchannels. **e** Variation of the openness of distributing and collecting channels

200–300 cm^{-1}, we chose to cut between 30 and 40 microchannels/cm. To avoid dead volumes in the electrolytic compartment, the overall dimensions of the distributing and collecting channels must be minimized. In addition the influence of their openness on the residence-time distribution of the flow constitutes the main goal of a study recently published [2], and of which the mains lines are summarized below:

An approached simulation (performed using Scilab software): the distributing and collecting channels are assumed to be a sequence of short segments of length L and with a rectangular cross-section. For each segment Poiseuille's law (1) is applied to evaluate the pressure drop ΔP (related to the corresponding flow Q_v).

$$\Delta P = Po\, 2\mu l\, Q_v / \mathrm{SD}_h^2 \tag{1}$$

The Poiseuille number for a rectangular cross-section can be calculated [5] from the following polynomial Eq. (2):

$$Po_R = 24\left(1 - 1.3553\, r_R^* + 1.9467\, r_R^{*2} + 1.7012\, r_R^{*3} - 0.9564\, r_R^{*4} - 0.2537\, r_R^{*5}\right) \tag{2}$$

where $0 < r_R^* < 1$ is the aspect ratio of the rectangular section defined by the depth:width ratio.

The main assumption for this simplified approach is that the outlet pressure of each segment of the distributing channel is assumed to be the same to the pressure at the inlet of the corresponding microchannel (Fig. 2a); in the same way, the outlet pressure of each microchannel is assumed to be the same to the pressure at the inlet of the corresponding segment of the collecting channel (Fig. 2a).

For instance, in the case of an electrode with ten microchannels, the system to solve contains 32 equations (11 for the distributing channel, 10 for the microchannels, and 11 for the collecting channel). The results give the optimal opening angle θ of the distributing and collecting channels (Fig. 2b) to allow uniform distribution of flow between the microchannels, (Fig. 3).

A rigorous treatment was performed by CFD calculations (Fluent), solving the Navier–Stokes equations, and the results [2] lead to "accurate" velocity and pressure drop profiles within the microstructured electrode. This rigorous approach requires long calculation times, so a more rapid hybrid model was prepared: the distributing and collecting channels are simulated by CFD calculation, while the reaction microchannels are simulated by the

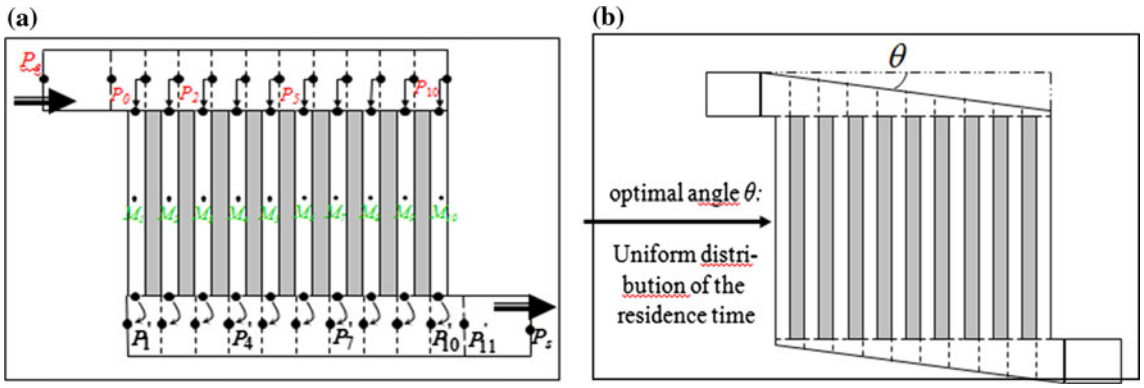

Fig. 2 Schematic representation of the microstructured electrode; chosen example: 10 reaction microchannels; Length: 5 mm for "micro-", "collecting-", and "distributing-" channels; depth: 50 µm for "micro-", "collecting-", and "distributing-" channels; width of microchannels: 250 µm; width for collecting and distributing channels 1 mm. **a** A possible non-optimized geometry. **b** Optimized geometry by variation of the opening angle θ of the distributing and collecting channels [2]

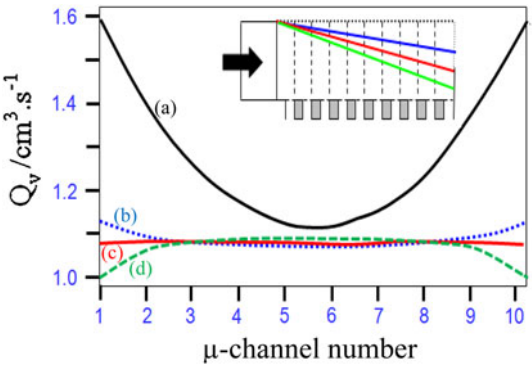

Fig. 3 Influence of the opening angle θ of distributing and collecting channels on the volume flow rate distribution within the microstructured electrode (described in Fig. 2). **a** $\theta = 0°$. **b** $\theta = 10.3°$. **c** $\theta = 10.6°$. **d** $\theta = 10.9°$

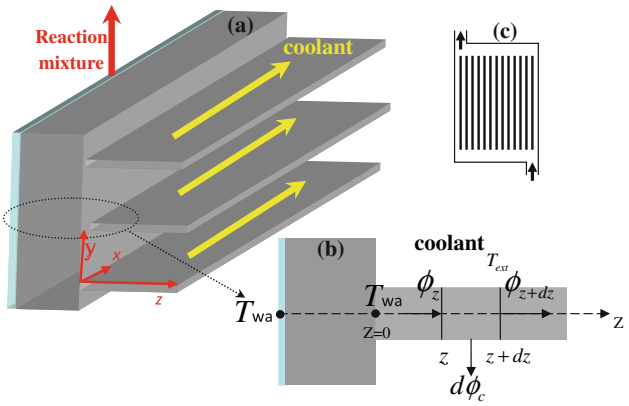

Fig. 4 Schematic representation of the heat exchanger to optimize (**a**), and thermal balance across a fin of length dz (**b**), flat projection of the heater (**c**). T_{wa} temperature of the block; ϕ_z heat flux across section at z and $d\phi_c$ heat exchanged by convection

analytical approach, where the phenomena are well known. This hybrid approach, allowing refinement of the mesh in the complex sections of the flow, provides more accurate data than the simple CFD approach, for the same computational effort. The agreement between analytical data and results from hybrid simulation is good, with a mean deviation of the flow rate of less than 4 %.

2.1.2 *Heat exchanger associated with microstructured electrode*

A steady-state thermal balance was performed to define the area required for a heater to provide rapid removal (or supply) of heat for exo/endo thermic reactions; the main idea is to facilitate heat transfer between the reaction area and a coolant. Two kinds of electrodes are examined:

(a) Platinum-covered microstructured silicon wafers. In this case, because of the fragility of the silicon wafer, a Teflon block was used as a backing support as well as for the tank containing the heat-exchange liquid. No specific estimation of the performance of this heat exchanger was performed.

(b) Microstructured flat metal fins (e.g., platinum and gold) soldered to a copper block with a "high area" heat exchanger on the back. The heat exchanger used was composed of a series of long thin rectangular fins dipped into a tank containing a flow of coolant (Fig. 4). The fins are parallel to the coolant flow, and perpendicular to the reaction mixture flow.

A thermal balance taking into account the fluorination reaction enthalpy, as well as the electrochemical irreversibilities (ohmic drop), is required to estimate the exchange area, i.e., the number and the size of fins, as a function of the operating parameters (e.g., volumetric flow, conversion, reagent concentration, coolant temperature, etc.), in order to operate, at steady state, under isothermal conditions within the electrolytic compartment.

The target reaction chosen in order to design and manufacture the heat exchanger (determination of the exchange area) was the fluorination of 2-deoxy-D-glucose (DG) leading to 2-fluoro-2-deoxy-D-glucose (FDG).

$$\mathrm{DG} + \mathrm{F_2} \rightarrow \mathrm{FDG} + \mathrm{HF} \quad (3)$$

Taking into account the bond energies of the molecules involved, the formation enthalpies of various atoms in the gas phase, and finally using thermodynamic cycles, it is possible to access the reaction enthalpy [3], by calculation of formation enthalpies of all reagents ($\Delta_f H^\circ_{\mathrm{DG\,C_6H_{12}O_5}} = -746.9$ kJ·mol^{-1}; $\Delta_f H^\circ_{\mathrm{FDG\,C_6H_{11}FO_5}} = -956.59$ kJ·mol^{-1}; $\Delta_f H^\circ_{\mathrm{HF}} = -267.6$ kJ·mol^{-1}). The result (the enthalpy change for the fluorination reaction of the DG: $\Delta_R H^\circ = -477.2$ kJ mol^{-1}) indicates an exothermic reaction.

For an "open", assumed plug-flow, microreactor operating at steady state, the overall energy balance, based on the first law of thermodynamics, can be written as follows:

$$\begin{aligned}&\text{Output enthalpy} - \text{input enthalpy}\\ &= \text{mechanical energy} + \text{electrical energy}\\ &\quad + \text{thermal energy}\end{aligned} \quad (4)$$

By introducing the converted flux F_c (mol·s^{-1}) the energy balance can be written as follows:

$$\begin{aligned}&F_c(\text{output enthalpy} - \text{input enthalpy})\\ &= \text{mechanical power} + \text{electrical power}\\ &\quad + \text{thermal power}\end{aligned} \quad (4a)$$

By expressing the enthalpy using Kirchhoff's law, and operating under isothermal conditions, the first term of this equation can be simplified to the reaction enthalpy (corresponding to the converted flux of the limiting reactant).

$$\sum_{\text{products}-\text{reactants}} v_j C_{p,j}\,\mathrm{d}T = 0 \tag{5}$$

for reactions under "isothermal conditions".

Consequently, in the absence of mechanical energy and assuming no influence of the pressure in the reaction enthalpy change, the overall energy balance (expressed in J s^{-1} or W) can be written:

$$\begin{aligned} F_c\Delta_R H = &\text{ electrical power } + \text{ exchanged heat flux} \\ \Rightarrow Q_v\Delta_R H\, C_0 X &= i S_a \Delta V + E_{\text{exch.}} \end{aligned} \tag{6}$$

where ΔV is the cell voltage, i the current density, and S_a the electrode area; X is the conversion during operating time (here the residence time τ); Q_v is the volumetric flow rate and C_0 the initial molar concentration of the reactant.

Assuming that the microreactor operates in galvanostatic "optimal" conditions (i.e., $I_{\text{applied}} = I_{\text{limiting}}$), the conversion rate X can be expressed according to:

$$X = 1 - \exp\{-S_a k/Q_v\} \tag{7}$$

where k is the mass transfer coefficient.

To evaluate the area required for the heat exchanger, it is necessary to establish the temperature profile between the bottom of the fin ($z = 0$) and the coolant; this profile gives access to the exchanged energy E_{exch}. To do this, some assumptions will be made:

- The reaction mixture must remain within the microchannels at constant temperature.
- The maximum temperature difference allowed between the inlet and the outlet of the coolant is 10 °C.
- Copper was used as material to construct the heat exchanger because of its good thermal conductivity; consequently we assume that the heat flux density received by the copper block is the same for any position on axes x and y. Consequently the temperature of the block is equal in any position ($x, y, z = 0$) and noted T_{wa}. Thermal transfer limitations are due to the metal fins.
- The total area of the fins has to be ~95 % of the area of the copper block bottom in contact with the coolant.

Taking into account the heat flux ($\phi_z(Z)$) across section z, as well as the heat exchanged by convection ($\mathrm{d}\phi_c$), the thermal balance for segment $\mathrm{d}z$ of the fin (Fig. 4) can be written according to Eq. (8).

$$\begin{aligned} \lambda S_{\text{exch}}\left\{\left(\frac{\mathrm{d}T}{\mathrm{d}z}\right)_{z+\mathrm{d}z} - \left(\frac{\mathrm{d}T}{\mathrm{d}z}\right)_z\right\} &= h p_{\text{exch}} \mathrm{d}z (T_z - T_{\text{ext}}) \\ \Rightarrow \frac{\mathrm{d}^2T}{\mathrm{d}z^2} - \frac{h p_{\text{exch}}}{\lambda S_{\text{exch}}}(T - T_{\text{ext}}) &= 0 \end{aligned} \tag{8}$$

In the case of rectangular fins with constant cross-section and heat transfer at the end of the fins, the boundary conditions can be written as: $T_{z=0} = T_{wa}$ and $-\lambda S_{\text{exch}}\left(\frac{\mathrm{d}T}{\mathrm{d}z}\right)_{z=L_{bl}} = h S_{\text{exch}}(T_{z=L_{bl}} - T_{\text{ext}})$

Solving (8) provides the temperature profile T (Eq. 9):

$$\frac{(T_z - T_{\text{ext}})}{(T_{wa} - T_{\text{ext}})} = \frac{\cosh(\omega(L_{bl} - z)) + \frac{h}{\omega\lambda}\sinh(\omega(L_{bl} - z))}{\cosh(\omega L_{bl}) + \frac{h}{\omega\lambda}\sinh(\omega L_{bl})} \tag{9}$$

where S_{exch} is the total area of all fins, T, T_{wa}, and T_{ext} the local temperature, blade wall temperature, and temperature far from the fin, p_{exch} the overall perimeter of the fin section, h the convective exchange coefficient of the coolant (here 507 W m^{-2} K^{-1}), λ the thermal conductivity of the coolant, $\omega : \sqrt{\frac{h p_{\text{exch}}}{\lambda S_{\text{exch}}}}$

The heat flux $\phi_{th} = -\lambda\, S_{\text{exch}}\, (\mathrm{d}T/\mathrm{d}z)_{z=0}$, i.e., the $E_{\text{exch.}}$, exchanged between the coolant and the fin (of which the length is L_{bl}) can be written according to Eq. (10):

$$\phi_{th} = \omega\lambda S_{\text{exch}}(T_{wa} - T_{\text{ext}})\tanh(\omega L_{bl})\frac{\tanh(\omega L_{bl}) + \frac{h}{\omega\lambda}}{1 + \frac{h}{\omega\lambda}\tanh(\omega L_{bl})} \tag{10}$$

Taking into account the conditions of these experiments:The exchange convective coefficient h of the coolant (ethylene glycol EG) was estimated using Nusselt's correlation:

$$\begin{aligned} Nu = h * L_{bl}/\lambda &= \text{constant}\; x\, Re^{0.5} Pr^{0.33} \\ &= 0.664(\rho L_{bl} u_{EG}/\mu)^{0.5}(C_p\mu/\lambda)^{0.33} \end{aligned} \tag{11}$$

where ρ the specific gravity (1109 kg·m^{-3}), μ the dynamic viscosity (0.02 Pa s), C_p the heat capacity (2.4 kJ·kg^{-1}·K^{-1}), and u_{EG} the coolant velocity (0.02 m·s^{-1}).

In these conditions, and considering $L_{bl} = 0.1$ m, the Nusselt's value was estimated to be 39.

For long ($L_{bl} \geq 0.1$ m) thin ($e_{bl} \leq 1$ mm) metal fins, the heat flux exchanged between the coolant and the fin can be simplified as follows:

$$\phi_{th} = E_{\text{exch}} = \omega\lambda S_{\text{exch}}(T_{wa} - T_{\text{ext}})\tanh(\omega L_{bl}). \tag{12}$$

This equation is used in the energy balance (6) to lead to the final energy balance Eq. (6b) allowing evaluation of the heat exchanger area.

$$\begin{aligned} 0 = &I S_a \Delta V - Q_v \Delta_R H\, C_0(1 - \exp(-S_a k/Q_v)) \\ &+ \omega\lambda S_{\text{exch}}(\tanh(\omega\lambda))(T_{wa} - T_{\text{ext}}). \end{aligned} \tag{6b}$$

The cell voltage term (ΔV), corresponds to irreversibilities (overvoltages) and ohmic drops; its value, was estimated by:

- Current–potential curves plotted using a rotating disk electrode as working electrode, under various conditions. The main factor varied was the concentration of fluorination agent [3].

– Resistance measurements of the solution and the separator between the anodic and cathodic compartments (the overall resistance for the microreactor estimated at 223 Ω).

Typical values of the electrochemical term ($I\ \Delta V$) were between 0.5 and 2 W for a geometrical area of the electrode of about 10 cm^2 and relatively high reagent concentrations (from 0.5 to 1 mol l^{-1}).

The value of the chemical term (changes in enthalpy) was 20–30 W for similar reagent concentrations, volumetric flows lower than 5 $cm^3\ min^{-1}$, and high conversion values ($X > 85$ %). Consequently, for electrochemical microreactors with an electrode geometrical area of $\sim$10 cm^2, the corresponding power to be removed by the coolant is about 20–30 W and the surface area of the heat exchanger (S_{exch}) has to be at least 5 cm^2. Note that this value covers uncertainties (one to two times the expected value) due to various approximations in the calculations.

2.2 Microreactor construction

Two different ways were used in this study to prepare the microstructured electrodes. First, soft lithography was used to groove a silicon wafer (Fig. 5a) with 150 rectangular-section microchannels with an opening angle for inlet/outlet channels of $\theta = 3.7°$. A $\sim$5 μm platinum layer was deposited by PVD on the microstructured wafer. However, poor adhesion of the platinum on the silicon/chromium significantly reduces the practical utility of the systems as electrosynthesis anodes.

Micro/nano-scratch (micro/nano-indentor) device, with a homemade needle, was used to create semi-ellipsoidal microgrooves on a gold and platinum plate. The excess metal accumulated at the microchannel sides was removed by polishing, and a satisfactory shape of microchannels was obtained (Fig. 5b).

The main idea was to allow easy heat transfer between the reaction area and the coolant. When the electrodes were microstructured metal plates, the electrode (platinum, gold) was soldered to a copper block with a heat exchanger on the other side. The heat exchanger was composed of several long thin metal fins dipped in a tank in which coolant flowed, as indicated in Fig. 5c, d. The fins were parallel to the coolant flow, and perpendicular to the reaction mixture flow.

The microchannel area was not perfectly smooth; nevertheless, the presence of microscopic holes/roughness (depth of holes/depth of microchannels <3 %) within the microchannel is beneficial to mass transfer. On the final electrode (Fig. 5d) there were 152 semi-ellipsoidal microchannels, with $\theta = 4.8°$ and specific area $S_a/V_{EC} \sim 210\ cm^{-1}$.

The micromechanically prepared heat exchanger (Fig. 5c) with its thirteen fins had a global area of 52 cm^2 (ten times the required area for the current application).

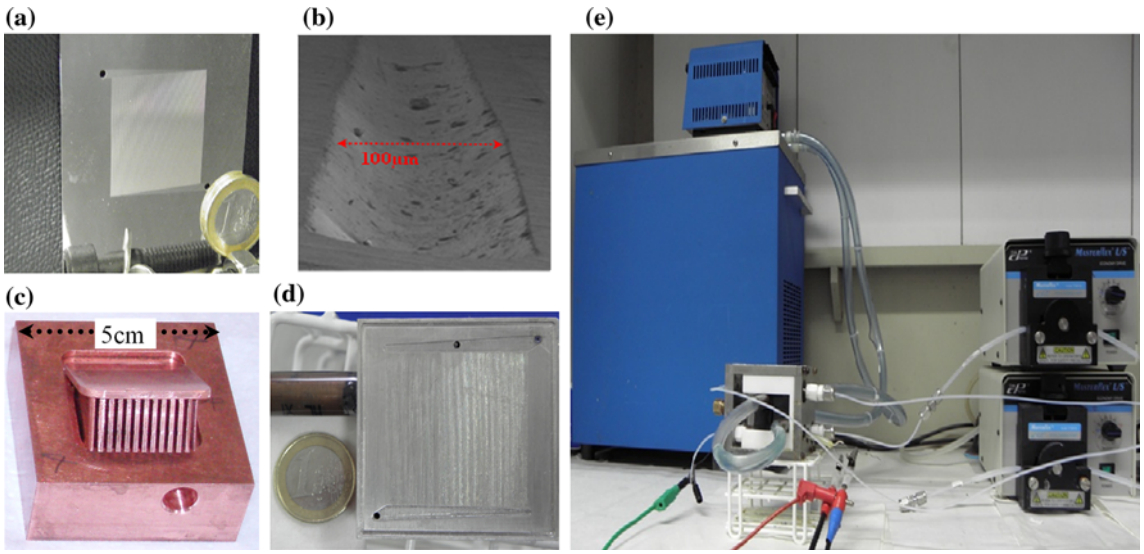

Fig. 5 Pictures of the microstructured electrodes and heater. **a** Microstructured silicon wafer, covered with platinum and containing $n_\mu = 150$ microchannels. **b** An "increasing size" microgroove, made using a microindentor. **c** Heat exchanger (13 fins, total surface area of 52 cm^2). **d** Integrated block contains the copper heat exchanger and the microgooved platinum electrode (152 semi-ellipsoidal microchannels cross-section: length: 35 mm; depth: 50 μm; width: 150 μm; microchannels overall geometrical area = n_μ*π*length*{(depth)^2 + (width)^2}$^{0.5}$/2 = 13.2 cm^2; microchannels overall volume = n_μ*π*length* (depth/2)* (width/2)/2 = 0.062 cm^3; the width of the distributing/collecting channels decrease from the inlet ($\sim$3 mm) to the outlet ($\sim$0 mm); $S_a/V_{EC} \sim 210\ cm^{-1}$). **e** Preparative electrolysis set-up

This fin area would allow a very large range of applications for instance solutions with higher concentrations and flow rates, as well as more exothermic reactions.

3 Microreactor for electrosynthesis: experimental results

The microstructured electrodes/heat exchanger block (Fig. 5d) was included in the microreactor (Fig. 5e) to perform electrosynthesis in two different ways: organic media for anodic fluorination reactions and aqueous media for enzymatic and "electrochemically assisted" chiral syntheses.

3.1 Anodic fluorination in the microreactor: fluorination of deoxy glucose in dimethoxy ethane and acetonitrile

The target molecule, deoxy-glucose, was studied in two solvents: acetonitrile and dimethoxyethane. The goal here was to carry out the reaction without risks (gaseous fluorine), in one electrochemical step instead of several chemical synthesis steps [requiring protection of the OH groups before fluorination in a second-order nucleophilic substitution, as described by reaction (13)] [6]. Moreover, the use of the heat exchanger allows fast heat transfer and better chemical selectivity.

Various fluorination agents (e.g., $(CH_3CH_2)_3N*3HF$ noted TEAHF, CsF, HF) were tested to carry out this reaction. The current–potential curves (curve 1, Fig. 6), obtained with the most appropriate fluorination agent, TEAHF in acetonitrile [7], shows two waves. The first (0.5–1.5 V) is due to the oxidation of the adsorbed TEAHF on the electrode and the second (1.5–2.7 V) corresponds to the oxidation of free TEAHF in solution [3, 7]. Curve 2 indicates low current for DG oxidation (signal from 1.2 to 1.8 V). Because of the low solubility of this substrate in acetonitrile, we were unable to rigorously compare curves 1 and 2, and could not conclude on the electrochemical activity of DG which seems very low. Nevertheless, it seems obvious that the fluorination agent TEAHF was oxidized before the deoxy-glucose.

Preparative electrolysis was carried out under various conditions to perform fluorination of DG in DME, CH_3CN and a mixture of the two. Fluorination was followed using ^{19}F NMR spectroscopy. The results, (^{19}F NMR) show that both the substrate (DG) and the solvent (DME) were fluorinated. This was surprising as DME seemed difficult to fluorinate. However, Hou and Fuchigami [8] reported fluorination of DME, and proposed a reaction scheme (Reaction 14), using F^- supplied by various forms of TEAHF (Et_3N*3HF, Et_3N*5HF Et_4N*3HF Et_4N*5HF) in acetonitrile; this reaction could lead to two isomers.

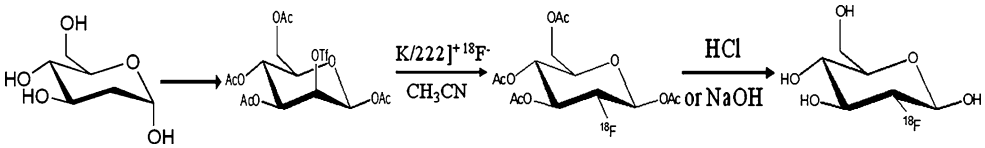

(13)

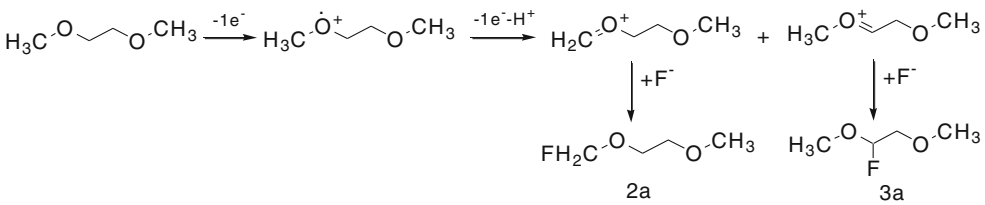

(14)

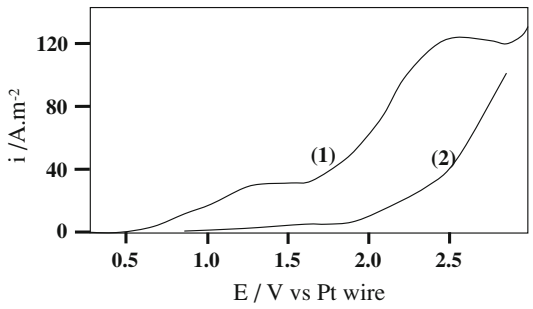

Fig. 6 Current potential curves obtained on platinum microstructured anode (Fig. 5d) within the microreactor presented in Fig. 5e. Solvent: CH_3CN; cathode: Pt; 25 °C. Anolyte flow = catholyte flow = 1 cm^3 min^{-1}. $r = 100$ mV s^{-1}. (*1*) $(CH_3CH_2)_3N$ 3HF 0.05 mol l^{-1}. (*2*) 2-deoxy-D-glucose 0.005 mol l^{-1} with $(CH_3CH_2CH_2CH_2)_4NClO_4$ 0.1 mol l^{-1}

The results of this study are listed in Table 1. NMR yielded four peaks at −136, −137, −151, and −154 ppm on the horizontal axis. The peak at −111 ppm was used as reference (sodium fluorobenzoate) [3]. Fine analysis of the NMR spectra did not indicate compounds containing two fluorides on the same carbon. Compound **2a** was found to be the majority product because fluorination of the methyl group is easier than fluorination of the methylene function. Difluorinated products such as $FH_2COCH_2CH_2OCH_2F$ (**2a′**) and $H_3COCHFCH_2OCH_2F$ (**3a′**) were also obtained.

For high values of the charge Q (runs 1–3), decreasing the temperature caused the selectivity for **2a** and **2a′** to increase. Similar results were obtained for lower charges (runs 4–6), Table 2.

Runs 1–7 were carried-out with 2-deoxy-D-glucose, while runs 1′–7′ were performed without.

The expected fluorination of the DG (DG is indicated as: –CHOH–CH_2–CHOH–) can be written as follows:

$$\begin{aligned} &-\mathrm{CHOH}-\mathrm{CH_2}-\mathrm{CHOH}- + \mathrm{F^-} \rightarrow \mathrm{H^+} \\ &\quad + 2\mathrm{e^-} + -\mathrm{CHOH}-\mathrm{CHF}-\mathrm{CHOH} \\ &\quad -(1-\mathrm{FDG}) \quad \text{and/or} \quad -\mathrm{CHOH}-\mathrm{CH_2}-\mathrm{CFOH} \\ &\quad -(2-\mathrm{FDG}) \end{aligned} \tag{15}$$

NMR results for runs 1 and 2 showed the presence of a peak at −184 ppm, close to the peak of commercial 2-FDG (−200 ppm). This means that the DG was fluorinated, but not at the expected position (2-FDG). We were not able to identify the exact formula of the reaction product, and CsF was not retained as fluorinating agent. Similar behavior was observed for runs 5 and 6, where the peak at −192 ppm corresponded to the expected 2-FDG. Note that a temperature decrease has a negative effect on the 2-DG fluorination; indeed, runs 3 and 7 carried out at −10 °C did not indicate the presence of 2-FDG. This result is surprising because numerous authors indicate the exothermicity of the fluorination reaction, and the opposite behavior was expected. On the other hand, NMR analysis showed the presence of peaks from −135 to −170 ppm, which were attributed to the CsF, or to adducts of the DME fluorination, as well as Et_3N–3HF decomposition adducts. Note that for all experiments the ratio "supplied amount of charge:required amount of charge" was higher than 1 and reached 18.5 in electrolyses 5–7.

To sum up, the microreactor allowed fluorination of 2-deoxy-D-glucose in one step although the overall process needs optimization, mainly fluorinating agent separation and 2-fluoro-2-deoxy-D-glucose purification. The electrical consumption, even though in excess, remained low, in comparison with the cost of the adduct produced.

3.2 NADH: continuous electroenzymatic regeneration

Many dehydrogenation reactions involve the use of the pyridinic cofactor NADH for the synthesis of optically active compounds. Because of the high cost of NADH (70 €/g), its regeneration constitutes an economic challenge. As far as we know, no industrial process allowing continuous in situ regeneration of this cofactor exists. Many electrochemical studies have reported indirect electrochemical synthesis of NADH using various redox mediators [9, 10]. Here, the electrochemical microreactor we designed was used in the

Table 1 Preparative electrolyses for dimethoxyethane fluorination within microreactor

Run	DME (mol l^{-1})	Et_3N–3HF (mol l^{-1})	*I*/mA	*t*/min	*Q*/*F* mol^{-1}	*T*/°C	Yield (%) of the fluorinated products/δ (ppm)			
							Monofluorinated **2a**/−151	Monofluorinated **3a**/−136	Difluorinated **2a′**/−154	Difluorinated **3a′**/−137
1	0.012	0.1	25	60	7.77	15	18	10	21	1
2	0.005	0.025	11	120	7.14	−5	27	5	30	0
3						−10	27	5	29	0
4	0.011	0.02	11	60	3.73	15	10.2	2.5	6.4	0
5						5	10.9	2.3	7.8	0
6						−5	10.5	2.3	8.7	0

Anode and cathode are made of platinum; solvent CH_3CN. Anolyte flow = catholyte flow = 0.2 cm^3 min^{-1}

Table 2 Preparative electrolyses for 2-deoxy-D-glucose (DG) fluorination within microreactor

Run	DG (mol l^{-1})	CsF (mol l^{-1})	*I*/mA	*t*/min	*Q*/*F*constructed microreactor (152 microchannels (mol^{-1})	*T*/°C	Fluorinated adducts other than deoxyglucose/ δ (ppm)	Fluorinated adduct from deoxy glucose/δ (ppm)
1	0.005	0.01	25	120	18	25	−138	−184 ppm
2						40	−138	−184 ppm
3						−10	−138, −152	–
4	0.005	–	10	50	3	40	−168 Et_3N–3HF −135 DME	–
4′	–							–
5	0.005		50	60	37	25	−135, −151, −154	−192
5′	–						−135, −151, −154, −176	–
6	0.005					40	−135, −151, −154	−191
6′	–						−151, −154	–
7	0.005					−10	−135, −151, −154,−168 (low magnitude)	–
7′	–						−151, −166	–

Runs 1–3 10 ml of TBAP 0.1 M in CH_3CN (90 %) with CH_3OH (10 %), *Runs 4–4′* 10 ml of CH_3CN (20 %) with DME (80 %), *Runs 5–8* 5 ml of CH_3CN (20 %) with DME (80 %). Anolyte flow = catholyte flow = 1 cm^3 min^{-1}, *Et_3N–3HF* 0.25 mol l^{-1}

$\delta = -200$ ppm obtained in the ^{19}F NMR spectra for commercial FDG within the binary solvent CH_3CN-90 %/CH_3OH-10 %

$\delta = -138$ ppm obtained in the ^{19}F NMR spectra for commercial CsF within the binary solvent CH_3CN 90 %/CH_3OH 10 %

continuous synthesis of chiral lactate (reaction χR 18) from achiral pyruvate, using electrogenerated NADH (reactions ER 16 and χR 17) Scheme 1.

In previous works [9] a theoretical simulation was performed with Comsol Multiphysics TM software, to propose a theoretical model for the microreactor by taking into account the electrochemical reaction (ER 16) and both chemical reactions (χR 17 and χR 18).

Navier–Stokes Eq. (16) was coupled with steady-state convection-diffusion Eq. (17) to simulate the microreactor.

$$\rho\left(\partial\overrightarrow{v}/\partial t + \left(\overrightarrow{v}\nabla\right)\overrightarrow{v}\right) = -\overrightarrow{\text{grad}}p + \mu\nabla^2\overrightarrow{v} + \rho\overrightarrow{g} \text{ coupled with } \nabla\overrightarrow{v} = 0 \quad (16)$$

$$\text{Convection} - \text{diffusion equation for species } j : \nabla(-D\nabla c_j + c_j\overrightarrow{v}) = r_j \quad (17)$$

where r_j is the rate of homogeneous reactions occurring in the bulk: for species FAD, $FADH_2$, NAD^+, NADH, pyruvate and L-lactate, rates are, respectively, $r_{\chi R17}$, $-r_{\chi R17}$, $-r_{\chi R17} + r_{\chi R18}$, $r_{\chi R17} - r_{\chi R18}$, $-r_{\chi R18}$, and $r_{\chi R18}$. Migration terms are ignored because of the presence of a supporting electrolyte, i.e., phosphate buffer.

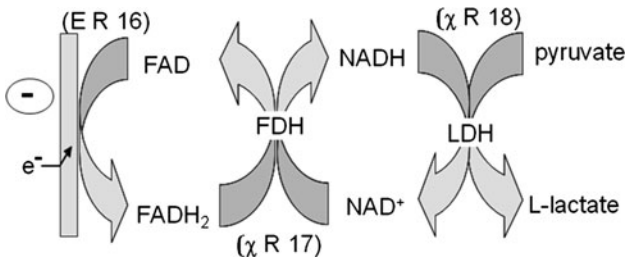

Scheme 1 Schematic representation of the enzymatic synthesis of L-lactate, involving indirectly electroregenerated NADH co-factor

The enzymatic reaction (χR17) between reduced flavin $FADH_2$ and nicotinamide adenine dinucleotide NAD^+ is an ordered reaction [9]; this means that there is a defined sequence of the reactions of the substrate NAD^+ with the enzyme FDH, first the NAD–FDH^+ complex appears, followed by a second "inhibition-reaction" providing the inactive NAD–FDH–NAD^{2+} complex. The kinetics of this system obeys Eq. (18):

$$r_{\chi R17} = \frac{k_{\text{cat}\chi R17} * [\text{FDH}]_\circ}{1 + K_{\chi R17} + \frac{K_{m\text{FADH}_2}}{[\text{FADH}_2]} + \frac{K_{m\text{NAD}^+}}{[\text{NAD}^+]}} \quad (18)$$

The enzymatic reaction (χR18) between reduced nicotinamide adenine dinucleotide NADH and pyruvate obeys an ordered Theorell–Chance mechanism; its kinetics can be modelled [9] as follows:

$$r_{\chi R18} = \frac{k_{\text{cat}\chi R18} * [L - \text{LDH}]_\circ}{1 + K_{\chi R18} + \frac{K_{m\text{NADH}}}{[\text{NADH}]} + \frac{K_{m\text{Pyruvate}}}{[\text{pyruvate}]}} \quad (19)$$

where $K_{m,j}$ is the Michaelis–Menten constants.

The equations are discretized by the finite-element method, and the expected results are the concentration profiles for various species as well as the conversion of reagents like NAD^+ and pyruvate. A further objective was to demonstrate the feasibility within the microreactor of the thermodynamically non-favoured reaction (χR17), leading

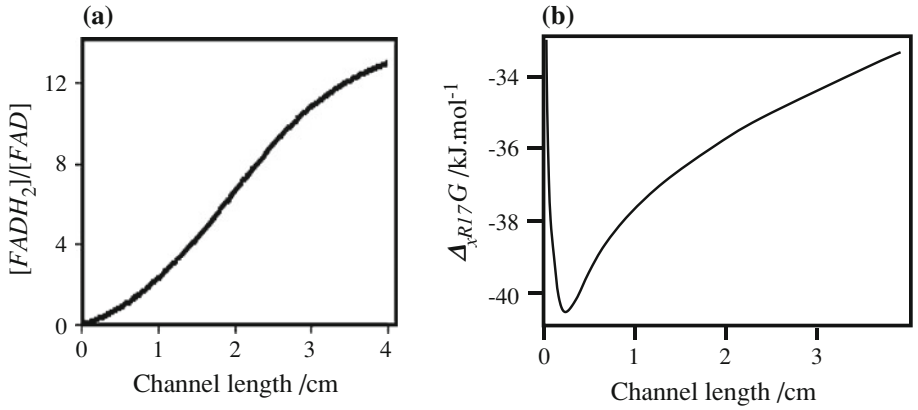

Fig. 7 Theoretical variation (Comsol Multiphysics TM software) of the simulated concentration ratio $[FADH_2]/[FAD]$ (**a**), as well as the changes in the free enthalpy $\Delta_R G$ of the chemical reaction $NAD^+/FADH_2$ (**b**), against the microchannel length, during electrolysis within the constructed microreactor (152 microchannels). $[FAD]_0 = 5$ mM; $[NAD^+]_0 = 3$ mM; $Q_{vanolyte} = Q_{vcatholyte} = 0.1$ cm^3 min^{-1}; $[FDH]_0 = 5$ U ml^{-1}. Enzyme free in solution

to the formation of the NADH, i.e., to demonstrate that, the regeneration of enzymatically active NADH using free enzyme in solution and electrochemically regenerated reduced flavin $FADH_2$ (ER 16), becomes thermodynamically possible within the microchannel, even though the change in its standard free enthalpy is positive $\Delta_R G^\circ_{\text{forward}\chi R17} = 20.3$ kJ mol^{-1}. Indeed, owing to the electrochemical regulation of the potential, operating in the restricted size (Fig. 5d) of the microchannels gives a high $[FADH_2]/[FAD]$ ratio (Fig. 7, $FADH_2$ is unstable in the bulk solution), which cause the sign of $\Delta_{\chi R17}G$ to become negative, and the forward χR17 to become spontaneous.

$$\Delta_{\chi R17} G = 20,300 + RT \ln \frac{[\text{FAD}] \cdot [\text{NADH}] \cdot [\text{H}^+]}{[\text{FADH}_2] \cdot [\text{NAD}^+]} \qquad (20)$$

The theoretical results show that conversion of FAD reaches about 95 %, but the $FADH_2$ produced was not consumed and its concentration at the outlet was about 14 times higher than the concentration of FAD. Experimental synthesis of L-lactate from achiral pyruvate was performed using lactic-dehydrogenase (LDH) and the results show that conversion of NAD^+ and pyruvate reached $\sim$40 and $\sim$20 %, respectively, for one residence time; this indicates that the electrochemical step is faster than the chemical reactions, which are the rate-limiting steps of the overall process. In these conditions, the flow rate and the temperature are the key parameters for optimization, in order to improve pyruvate conversion within the electrochemical microreactor.

Preparative electrolyses were performed under potentiostatic conditions using the filter press microreactor. $FADH_2$ produced at the gold cathode reacts chemically with NAD^+ to lead to NADH; then, L-lactate is synthesized by the action of the continuously electro-regenerated NADH on the pyruvate. The results show that in these conditions the maximum concentration of FDH, must not exceed 0.005 U cm^{-3} and for LDH the optimum value is 0.03 U cm^{-3}. The overall production rate of L-lactate can reach 0.13 mol m^{-2} day^{-1}, a relatively low value because of the low concentrations of NAD^+ and FAD used.

Nevertheless, the cost of formate dehydrogenase free in the solution limits the applicability of the process so the FDH was immobilised to reduce the quantity required [10]. The FDH was encapsulated within modified chitosan deposited on the microstructured face of the electrode, according to the following scheme (Scheme 2)

Formate was used to regenerate NADH to simplify the overall process (no electrochemical step); nevertheless, the same scheme can be used for NADH, electro-generated by mediation of the flavin cofactor.

Figure 8 reports the results obtained with FDH immobilized in chitosan and a solution flowing through the microreactor containing an excess of formate as well as the NAD^+. The FDH enzyme seems to keep more than the half of its initial activity over practically 3 weeks of continuous reaction. The same kind of experiment carried out with pyruvate led to L-lactate with over 60 % conversion [11]. Nevertheless, because of the limited quantity of FDH

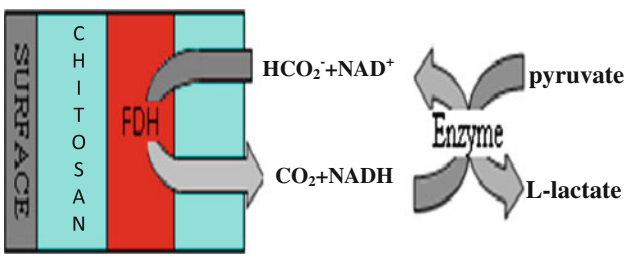

Scheme 2 Schematic representation of continuous NADH regeneration (and use for chiral synthesis), involving immobilized FDH enzyme within modified chitosan

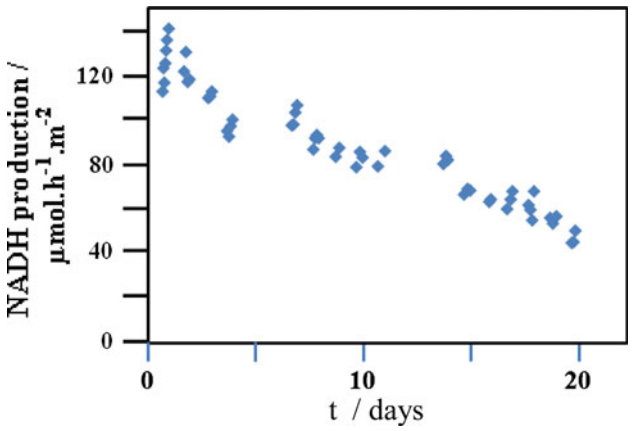

Fig. 8 Experimental production of NADH based on reaction Scheme 2. $[NAD^+]_0 = 5$ mol m^{-3}; $Q_{vanolyte} = Q_{vcatholyte} = 0.06$ cm^3 min^{-1}. Immobilized FDH = 230 U m^2, or 19.2 U g^{-1} of chitosan

immobilized, overall NADH production (and consequently the chiral adduct expected) remained low (0.0029 mol m^{-2} day^{-1}), namely 45 times lower than the quantities obtained with FDH free in solution.

4 Conclusion

Theoretical approaches carried out during this study allow the proposal of an optimized form of microstructured electrodes; the optimal value of the opening angle of the distributing and collecting channels, allowing uniform flow distribution, was determined as a function of the microchannel number. In addition, a heat exchanger with a surface area appropriate for fluorination reactions was designed, constructed and coupled to the microstructured electrode. The resulting microreactor was used for two applications (fluorination and chiral syntheses) with satisfactory results, i.e., improvement of selectivity and achievement of not-thermodynamically spontaneous reactions.

Acknowledgments We would like to thank P. Cognet from the LGC for his helpful discussions.

References

1. Renault C, Colin S, Orieux S, Cognet P, Tzedakis T (2010) Optimal design of multi-channel microreactor for uniform residence time distribution. In: Proceedings of the 2nd European conference on microfluidics—Microfluidics 2010, Toulouse, 8–10 Dec 2010
2. Renault C, Colin S, Orieux S, Cognet P, Tzedakis T (2012) Optimal design of multi-channel microreactor for uniform residence time distribution. Microsyst Technol 18:209–223
3. Renault C (2011) Développement de microréacteurs pour la synthèse de radio-traceurs pour l'imagerie médicale. PhD, University of Toulouse, Toulouse
4. Commenge JM, Falk L, Corriou JP, Matlosz M (2002) Optimal design for flow uniformity in microchannel reactors. AIChE J 48:345–358
5. Shah RK, London AL (1978) Laminar flow forced convection in ducts. Academic Press, New York
6. Hamacher K, Coenen HH, Stöcklin G (1986) Efficient stereospecific synthesis of no-carrier-added 2-[^{18}F]-fluoro-2-deoxy-D-glucose using aminopolyether supported nucleophilic substitution. J Nucl Med 27:235–238
7. Ciumag MR, Tzedakis T, André Barrès C (2012) Voltammetric behavior of triethylamine trihydrofluoride and anisole in acetonitrile as a first approach of studies for electro-fluorination of some adducts. Electrochim Acta 70:142–152
8. Hou Y, Fuchigami T (1999) Electrolytic partial fluorination of organic compounds. Part 37: selective electrolytic fluorination of dimethoxyethane, diethylene glycol dimethyl ether, and crown ethers. Tetrahedron Lett 40:7819–7822
9. Kane C, Tzedakis T (2008) Electrochemical microreactor for chiral syntheses using the cofactor NADH. AIChE 54(5):1365–1376
10. Roche J (2011) Régénération continue du cofacteur NADH catalysée par la formate deshydrogénase immobilisée en réacteur filtre presse. PhD, University of Toulouse, Toulouse
11. Roche J, Groenen Serrano K, Reynes O, Tzedakis T (2010) in: Nouveau procédé de régénération enzymatique continue de NADH et de détection de NAD^+ et système pour sa mise en œuvre. French patent N° BFF10P0105